Cryogenic Hydrogen Tanks via Additive Manufacturing and Laser Beam Welding in Vacuum

Benjamin Gerhards*[a], Frederik Diersmann[a], Christian Otten[a],

[a]LaVa-X GmbH, Kaiserstraße 100, 52134 Herzogenrath, Germany;

*corresponding author: gerhards@lava-x.de

Abstract

The “CHASMA – Cryogenic Hydrogen Tanks via Additive Manufacturing” project aims to demonstrate an innovative liquid hydrogen tank concept for emission-free aviation. Liquid hydrogen tanks operate under a pressure of approximately 4 bar. Thermally induced pressure increases result in "boil-off" gas, Hydrogen must be vented, which reduces efficiency. To minimize this, a multilayer vacuum insulation in a sandwich structure made of additively manufactured chromium-nickel steel is being developed. The individual segments of the resulting tank must be welded together. Laser beam welding in a vacuum combines the welding process and the creation of vacuum insulation in a single step. Trials with 2 mm thick stainless steel sheets, arranged at distances of 15 – 20 mm and welded, demonstrate the process feasibility. The results show a broad parameter range for three-sheet connections, enabled by both beam oscillation and Brightline technology.

Keywords: Laser welding, Laser welding in vacuum, LaVa, hydrogen cryo tank, multi layer welding

1 Introduction

Hydrogen is a versatile energy carrier central to the European Union’s “Green Deal” targets adopted in December 2019. According to the European Commission’s report “A hydrogen strategy for a climate-neutral Europe” [1], it offers cross-sectoral potential in buildings, industry, and transport. Hydrogen fuel cells emit neither CO_2 nor NO_x, and even combustion results in only minimal NO_x emissions, making hydrogen essential for decarbonizing hard-to-abate sectors [2].

Aerospace is one such sector, where replacing kerosene with hydrogen could substantially reduce climate impact. However, key challenges persist, including limited green hydrogen infrastructure and hydrogen's lower volumetric energy density—both as gas and cryogenic liquid—which necessitates larger storage volumes [3].

Liquid hydrogen must be stored at cryogenic temperatures, requiring high-performance thermal insulation. Heat ingress leads to pressure build-up and boil-off gas, which must be vented, reducing system efficiency and operational range.

The CHASMA research project (Cryogenic Hydrogen Tanks via Additive Manufacturing) addresses these challenges by developing an innovative lightweight tank design aimed at minimizing boil-off. The concept uses a multifunctional sandwich structure with alternating layers and lattice cores, joined via multilayer butt welding. To enable geometric flexibility and reduce tooling demands, the tank and insulation layers will be additively manufactured using Laser Powder Bed Fusion (LPBF) with fully austenitic stainless steel.

LaVa-X is responsible for developing the welding process for these multifunctional insulation layers. This study investigates multilayer butt welds using both conventionally and additively manufactured stainless steel, forming the technical basis for future hydrogen tank welding trials.

1.1 Laser welding in vacuum

Laser beam welding in vacuum (LaVa) is a innovative process. Compared to conventional Laser beam welding, it is characterised by an increase in process stability [4] with a simultaneous increase in quality (to the level of electron beam welds [5]) and penetration depth [6]. Conversely, this also means that a required penetration depth can be achieved with a significantly reduced energy requirement [7], which also correlates with a significant reduction in CO_2-emissions.

The advantages of the LaVa welding process arise from several physical phenomena. First, the vacuum environment significantly suppresses the vapor plume above the capillary, minimizing absorption and scattering of laser radiation [8]. Second, the vaporization temperature of metals decreases sharply under reduced pressure [9], lowering the capillary temperatures [10]. These effects enhance energy coupling into the material and reduce the lateral extension of the melt pool [11]. As a result, keyhole stability is markedly improved. While frequent collapse occurs under atmospheric pressure, the capillary remains stable in a vacuum [12]. LaVa welding enables high process stability

even at elevated power levels and low feed rates, where atmospheric welding typically leads to excessive spattering [13]. Furthermore, the vapor ejection is more uniform, resulting in a smoother weld surface [14].

In addition, the tendency to form pores is significantly reduced by the vacuum, as the capillary shape and melt pool flows are altered [15]. An upward flow forms behind the capillary, which means that gas pores, e.g. sheared from the capillary, can outgas from the weld pool [16]. While electron beam welding is considered unsuitable for mass production due to the vacuum required, Laser beam welding in a vacuum has the advantage that the process can be carried out in a rough vacuum of approx. 10^0-10^2 mbar [17].

2 Experimental Procedure

2.1 Experimental setup

The LaVa-Cell 450 from LaVa-X GmbH is used for the experiments, as it is suitable in terms of its modularity and available laser power. The system is equipped with an 8 kW Multimode disc laser from the TruDisk series by TRUMPF SE + Co KG [18]. The following Table 1 shows the relevant beam data of the LaVa-Cell 450 used.

Beam data TRUDisk 8000 MM with IPG wobbler D50			
	MM 50 µm (core fibre)	MM 200 µm (ring fibre)	unit
Laser wavelength	1030	1030	nm
M² In	6,1	24,4	-
MPP In	2,0	8,0	mm*mrad
Fibre In	50	200	µm
Fibre Out	50	200	µm
M² Out	6,1	24,4	-
Collimation length	150	150	mm
∅ on collimation lense	24	24	mm
Image ration	3,33	3,33	-
Focal length	500	500	mm
Focal diameter	166,67	666,67	µm
Rayleigh length	3,47	13,89	mm

Table 1: Beam data of LaVaCELL450

The column labeled "MM 50 µm" refers to the core fiber of the laser light cable (LLK) with a diameter of 50 µm. When TRUMPF BrightLine Weld (BLW) technology is used, the system incorporates an additional 200 µm ring fiber arranged concentrically around the core. Without BLW, only the 50 µm core fiber is utilized for beam delivery.

As shown in Figure 1, the vacuum chamber is equipped with x- and y-axes for precise sample positioning. A vacuum pump located beneath the chamber ensures continuous evacuation and removal of process by-products such as fumes and spatter. Laser radiation enters the chamber through a protective glass window, which also shields the optical system from contamination.

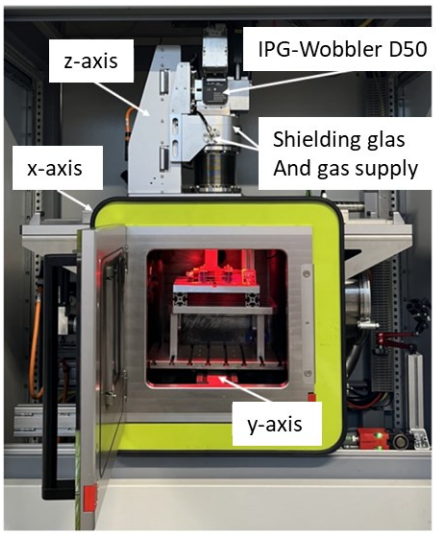

Figure 1: LaVaCELL 450

2.2 Material

Two materials were selected for the experimental investigations. The first is austenitic stainless steel 1.4301 (X5CrNi18-10), welded in specimens measuring 50 mm × 50 mm × 2 mm.

Based on initial welding trials with 1.4301, the process will be transferred to the preferred material, Voestalpine XM-19, tested in dimensions of 30 mm × 30 mm × 2 mm. XM-19 offers superior suitability for cryogenic environments down to −196 °C while maintaining high impact toughness. Additionally, its yield strength of 380 N/mm², nearly double that of 1.4404 stainless steel, makes it particularly advantageous for hydrogen tank applications.

2.3 Experimental procedure

The number of layers was fixed to three, with the laser beam focused on the top surface of the middle sheet. An initial interlayer spacing of 15 mm was applied.

For 2 mm thick stainless steel, effective parameters include a welding speed of 20 mm/s, an oscillation amplitude of 0.2 mm, and a frequency of 400 Hz. These values remained constant throughout the initial trials. At a laser power of 600 W, full penetration to a depth of ~2 mm was achieved.

Welding was performed under a vacuum pressure of 100 mbar. The shielding gas flow was set to 30 L/min of high-purity argon, slightly above standard, to counteract increased process emissions and reduce laser–vapor interaction. A schematic of the welding setup is presented in Figure 2.

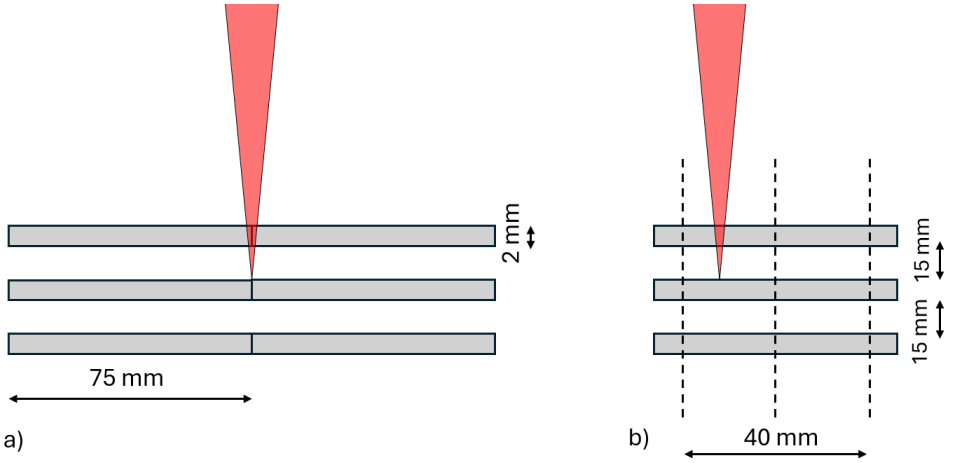

Figure 2: a) frontal view b) side view

As shown in Figure 2 a, the weld seam length is consistently 40 mm across all experiments. Each weld incorporates ramped power transitions at the start and end to stabilize capillary formation and prevent sudden collapse. The initial and final ramps measure 2 mm and 4 mm, respectively. The three weld layers are always arranged vertically, where the letters T = Top, M = Middle, and D = Down refer to the respective layers of the weld seam. This arrangement is consistent with the experimental setup.

The experimental campaign follows an iterative approach, where each parameter set builds on prior results. Three experimental series, labeled A, B, and C, were conducted. to establish an initial parameter set capable of producing acceptable weld quality at different conditions. At this stage, parameter optimization is not the primary focus.

The first series A systematically examines the influence of BrightLine Weld (BLW) technology and beam oscillation across four process variants as bead on plate welds:

1. Core welding without oscillation
2. BLW welding without oscillation
3. Core welding with oscillation
4. BLW welding with oscillation

Here, “core welding” refers to scenarios where 100% of the laser power is delivered through the central fiber. In contrast, “BLW welding” involves distributing a portion of the power (>0%) to the ring fiber.

Series A investigates all four configurations at a fixed interlayer distance of 15 mm.

The results from series A, are used to transfer the most promising parameter sets to series B, which is conducted with butt joint configurations. The primary aim is to investigate weld behavior for different bevel preparations, manufacturing processes and distances between the layers.

In series C, manufacturing tolerances like gaps and edge misalignments are investigated.

3 Results and Discussion

In the first set of experiments, welds were conducted without and with Brightline Weld, with a beam oscillation and with the combination of both. The parameters are displayed in Table 2.

#	P_L [W]	v_s [mm/]	C [%]	R [%]	A [mm]	F [Hz]
A-1	4400	20	100	0	0	0
A-2	5866	20	50	50	0	0
A-3	4400	20	100	0	0,15	400
A-4	5866	20	50	50	0,3	400

Table 2: Parameters of the first set of experiments, A

At a total power of 4400 W with full core intensity, complete penetration welding was achieved. In the D-layer of sample A-1, root notches were identified. Sample A-2, which has a lower core share as A-1, highlights the clear influence of the ring beam component. In the M-layer, the center of the weld is approximately 0.3 mm wider, and a ~100% increase in weld width is observed on the top side. This effect is also visible in the D-layer, where the hourglass-shaped weld geometry is more pronounced and broader than in sample A-1.

Parameter A-3 also used 4400 W of core power, but with an oscillation amplitude of 0.15 mm. Compared to A-1, this amplitude did not significantly affect the weld width in outer layers. The minimal width in the M-layer however was increased by 0.1 mm. All welds employing oscillation exhibited weld irregularities, mainly root notches, and additional bilateral undercuts in the D-layer. A similar but less pronounced effect was observed with the combination of beam shaping (BLW) and oscillation. In sample A-4, undercuts were also found in both the M- and D-layers. The center width in the M-layer was increased by 100 µm. Hence, the combination of oscillation with BLW technology is also suitable for the process.

The cross sections of the different weld samples are displayed in Figure 3.

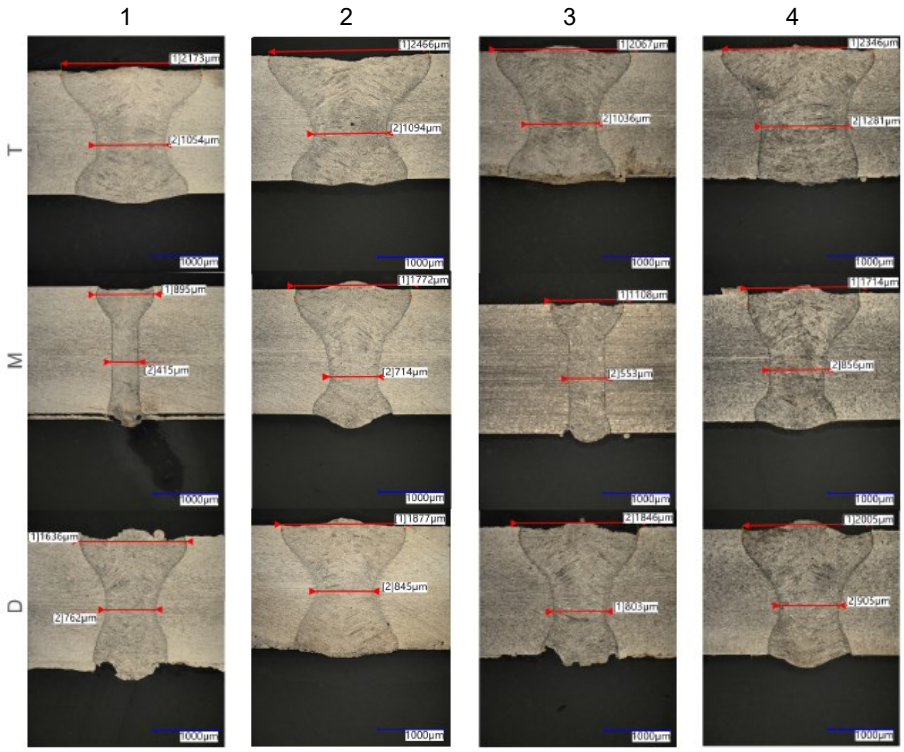

Figure 3: Cross sections of the first set of experiments, A

In the subsequent experimental series B, the welding process was applied to a butt joint configuration. The first two experiments (B-1 and B-2) employed identical parameters, incorporating both BLW and beam oscillation. In contrast, the third experiment (B-3) was conducted without oscillation, as detailed in Table 3.

#	P_L [W]	v_s [mm/]	C [%]	R [%]	A [mm]	F [Hz]
B	5866	20	50	50	0,3	400
B-1	Edges cut by impact scissors					
B-2	LBPF-generated “as built”					
#	P_L [W]	v_s [mm/]	C [%]	R [%]	A [mm]	F [Hz]
B	5866	20	50	50	0	0
B-3	20 mm distance between the three layers					

Table 3: Parameters of the second set of experiments, B

This distinction was made due to differences in joint preparation: B-1 and B-2 exhibited minor interfacial gaps resulting from bevel preparation, whereas in B-3, the joint edges were precision-milled to ensure a technical zero gap bevel preparation.

A total laser power of 2933 W was applied, resulting in complete penetration in all samples. In sample B-1, no irregularities were observed in the top (T) layer. However,

a root concavity was identified in the D-layer. Additionally, a pronounced undercut is present on the right side of the M-layer, which is presumably attributable to the joint preparation conducted by impact scissozrs.

Sample B-2 exhibited undercuts in both the T- and M-layers, while a root concavity was again detected in the D-layer. Compared to sample A-4, the characteristic hourglass-shaped weld profile is either significantly diminished or absent altogether, a condition likely influenced by the LPBF-manufacturing process that didn't ensure a zero gap bevel preparation.

In contrast, sample B-3, where the distances between the layers was 20 mm, revealed no observable welding irregularities such as undercuts or concavities. Moreover, the hourglass morphology is clearly pronounced in both the T- and D-layers. The weld width at the top surface is approximately 0.1 mm to 0.2 mm higher than that of sample A-4. The M-layer in B-3, by contrast, exhibits a geometry resembling an inverted conical shape. Despite this, the minimal weld seam width remains comparable to that observed in sample A-4.

The corresponding cross-sectional images are presented in Figure 4.

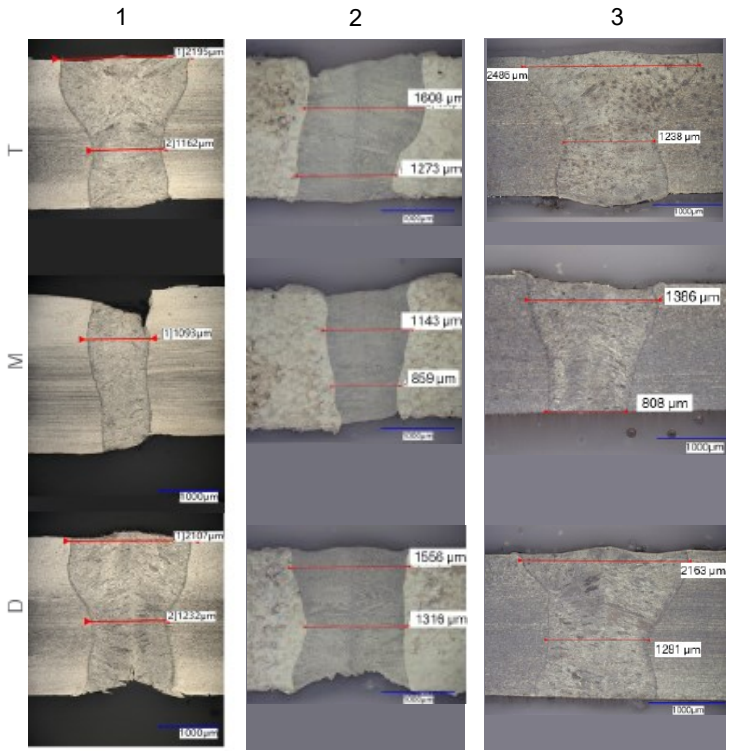

Figure 4: Cross sections of the second set of experiments, B

For the last set of experiments, manufacturing tolerances in form of gaps and edge misalignments were simulated. Therefore, a gap of 0.2 mm and an edge misalignment of 0.3 mm was adjusted. To achieve a better gap bridging ability, the BLW parameter

with additional beam oscillation as used for C-1, while C-2 was carried out with BLW, as the edge misalignment was adjusted in a technical zero gap, Table 4.

#	P_L [W]	v_s [mm/]	C [%]	R [%]	A [mm]	F [Hz]	bevel preparation
C-1	5866	20	50	50	0,3	400	0,2 mm gap
C-2	5866	20	50	50	0	0	0,3 mm edge misalignment

Table 4: Parameters of the third set of experiments, C

Given that the middle (M) layer exhibits the lowest weld width and is therefore the most critical with respect to joint integrity, only the corresponding cross-sections are shown in Figure 5.

In sample C-1, the M-layer reveals a surface concavity on the top side of the sheet, measuring approximately 120 µm. Additionally, a minor edge notch is present on the root side, located on the left.

By contrast, the M-layer of sample C-2 exhibits no welding irregularities aside from the inherent edge misalignment.

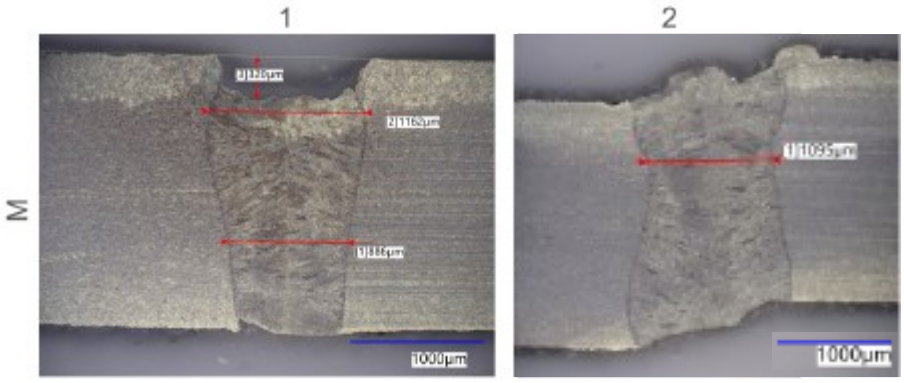

Figure 5: Cross sections of the third set of experiments, C

The conducted experiments showed that a multi-layer connection between three stainless steel sheets can be welded in a wide variety of conditions, such as bevel preparations, manufacturing technologies and manufacturing tolerances. While the formation of undercuts and convexities can be mitigated by optimized welding parameters, they cannot be completely avoided when gaps are formed within the joints. The M-layer exhibits the most critical one, as the minimal weld width is significantly smaller compared to the T- and D-layer.

4 Summary

The CHASMA research project aims to develop an innovative lightweight cryogenic hydrogen tank for zero-emission aviation. The concept employs a multilayer sandwich

structure with vacuum insulation, manufactured via Laser Powder Bed Fusion (LPBF) using austenitic stainless steel. To join the individual tank segments, laser beam welding in vacuum (LaVa) is applied, combining the welding process with vacuum encapsulation.

The experiments are conducted using a LaVaCELL 450 setup and TRUMPF's BrightLine Weld (BLW) technology, with optional beam oscillation. Three stainless steel sheets are welded in multilayer configuration under vacuum (100 mbar). The process is first tested on 1.4301 stainless steel and then transferred to XM-19, preferred for cryogenic use due to its strength and low-temperature toughness.

Four experimental series (A–C) evaluate combinations of core/ring power ratios, oscillation, gap tolerance, and focal positioning. The results demonstrate:

- A broad process window for multilayer joints
- The potential for gap-bridging and edge misalignment compensation
- Promising results for applying the technique to real tank geometries

The findings lay the groundwork for welding full-scale hydrogen tanks and suggest that laser welding in vacuum is a viable alternative to electron beam welding, suitable for high-quality, scalable production.

5 Acknowledgements

The project CHASMA (20W2211C) is funded by the Federal Ministry of Economic Affairs and Energy on the basis of a decision by the German Bundestag.

Supported by:

Federal Ministry
for Economic Affairs
and Energy

on the basis of a decision
by the German Bundestag

Data Availability Statement

Supporting Material are available in a separate file attached. The raw data that support the findings of this study are available from the corresponding author under the following link and upon reasonable request: *available after acceptance*

6 References

[1] N.N. Mitteilung der Kommission an das Europäische Parlament.: Eine Wasserstoffstrategie für ein klimaneutrales Europa. [July 08, 2025]; Available from: https://eur-lex.europa.eu/legal-content/DE-EN/TXT/?from=EN&uri=CELEX%3A52020DC0301.

[2] Leichler J, Giese A, Görner K. Wasserstoff als Dekarbonisierungsoption für Hochtemperaturprozesswärme -Auswirkungen auf die Bildung und Bewertung von Stickoxidemissionen. 4. Aachener Ofenbau- und Thermoprozess-Kolloquium 2023, 2023.

[3] N.N. Wasserstoff und sein Potenzial in der Luftfahrt. [July 08, 2025]; Available from: https://www.easa.europa.eu/de/light/topics/hydrogen-and-its-potential-aviation.

[4] Reisgen U, Olschok S, Jakobs S, Turner C. Laser beam welding under vacuum of high grade materials. Weld World 2016;60(3):403–13. https://doi.org/10.1007/s40194-016-0302-3.

[5] Börner C, Dilger K, Rominger V, Harrer T, Krüssel T, Löwer T. Influence of ambient pressure on spattering and weld seam quality in laser beam welding with the solid-state laser. In: International Congress on Applications of Lasers & Electro-Optics. Laser Institute of America; 2011, p. 621–629.

[6] Sokolov M, Salminen A. Methods for Improving Laser Beam Welding Efficiency. Physics Procedia 2014;56:450–7. https://doi.org/10.1016/j.phpro.2014.08.148.

[7] Otten C. LaVa-X Technologieberatung: Profitieren Sie von unserem Know How; Available from: https://www.lava-x.de/de/technologieberatung/laserschweissen-beratung.

[8] Luo Y, Tang X, Lu F, Chen Q, Cui H. Effect of subatmospheric pressure on plasma plume in fiber laser welding. Journal of Materials Processing Technology 2015;215:219–24. https://doi.org/10.1016/j.jmatprotec.2014.08.011.

[9] Jiang M, Tao W, Wang S, Li L, Chen Y. Effect of ambient pressure on interaction between laser radiation and plasma plume in fiber laser welding. Vacuum 2017;138:70–9. https://doi.org/10.1016/j.vacuum.2017.01.012.

[10] Pang S, Hirano K, Fabbro R, Jiang T. Modeling keyhole and weld pool dynamics of laser welding under variable ambient pressure. In: International Congress on

Applications of Lasers & Electro-Optics. Laser Institute of America; 2012, p. 685–694.

[11] Katayama S, Ido R, Nishimoto K, Mizutani M, Mizutani Y. Full penetration welding of thick high tensile strength steel plate with high-power disk laser in low vacuum. Welding International 2018;32(5):289–302. https://doi.org/10.1080/09507116.2017.1346776.

[12] Jiang M, Chen X, Chen Y, Tao W. Increasing keyhole stability of fiber laser welding under reduced ambient pressure. Journal of Materials Processing Technology 2019;268:213–22. https://doi.org/10.1016/j.jmatprotec.2019.01.026.

[13] Rominger V, Berger P, Hügel H. Effects of reduced ambient pressure on spattering during the laser beam welding of mild steel. Journal of Laser Applications 2019;31(4):42016. https://doi.org/10.2351/1.5007186.

[14] Luo Y, Tang X, Deng S, Lu F, Chen Q, Cui H. Dynamic coupling between molten pool and metallic vapor ejection for fiber laser welding under subatmospheric pressure. Journal of Materials Processing Technology 2016;229:431–8. https://doi.org/10.1016/j.jmatprotec.2015.09.048.

[15] Engelhardt T, Heider A, Weber R, Graf T. Time-resolved x-ray analysis of the keyhole behavior during laser welding of steel and aluminum at reduced ambient pressure. In: International Congress on Applications of Lasers & Electro-Optics. Laser Institute of America; 2015, p. 250–256.

[16] Jiang M, Chen X, Chen Y, Tao W. Mitigation of porosity defects in fiber laser welding under low vacuum. Journal of Materials Processing Technology 2020;276:116385. https://doi.org/10.1016/j.jmatprotec.2019.116385.

[17] Börner C, Fischer F, Dilger K. High quality laser welding by reducing the ambient pressure. In: International Congress on Applications of Lasers & Electro-Optics. Laser Institute of America; 2014, p. 926–932.

[18] N.N. Hochleistungsfestkörperlaser. [July 08, 2025]; Available from: https://www.trumpf.com/de_DE/produkte/laser/scheibenlaser/trudisk/.

[19] N.N. Wobbel-Schweißköpfe. [July 08, 2025]; Available from: https://www.ipgphotonics.com/de/products/beam-delivery/laser-processing-heads/wobble-welding-heads.